Chapter-III

Surfactants assisted synthesis of CuAl-sodium dodecyl sulfate layered double hydroxide and its adsorptive removal of methyl red dye from aqueous solution**.**

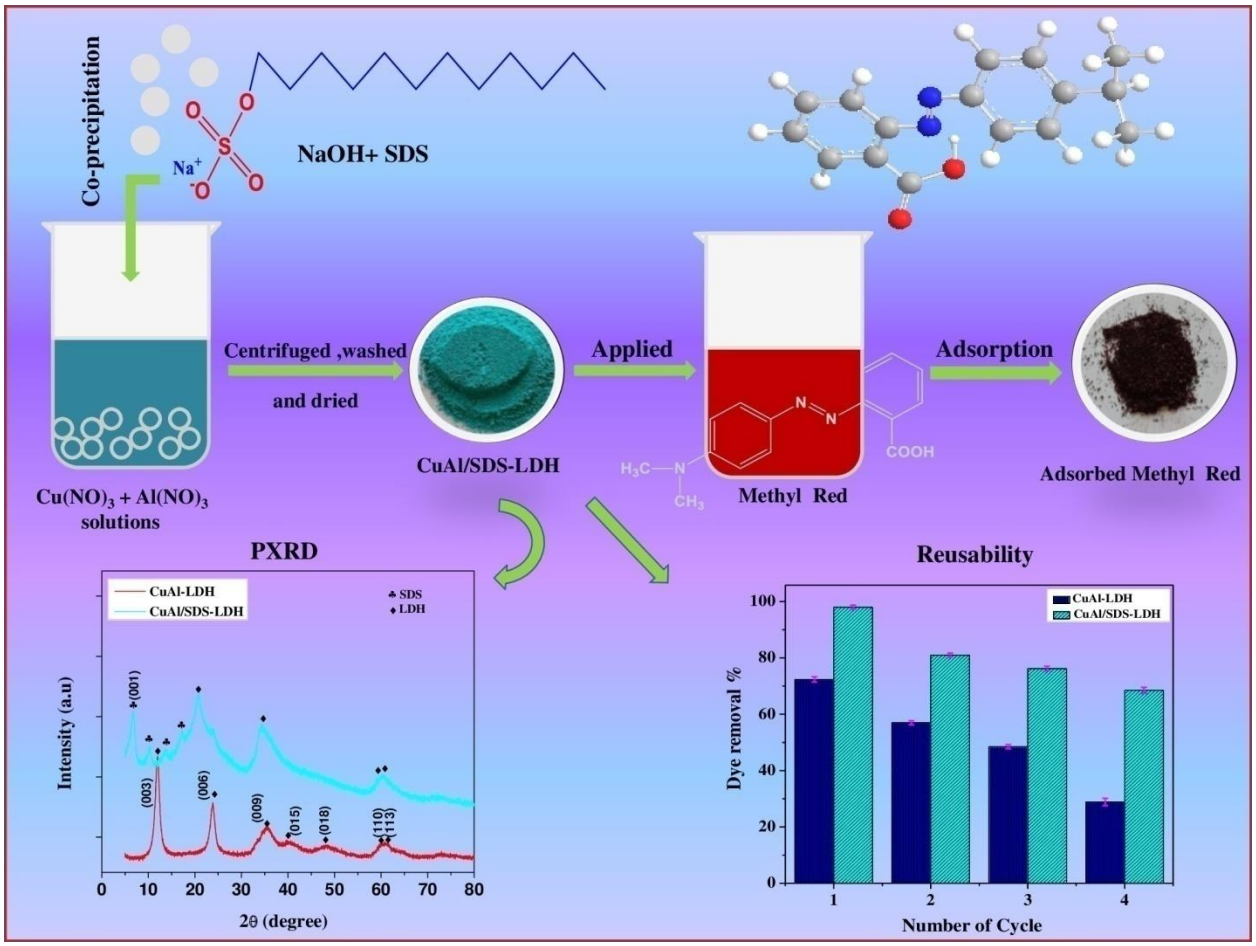

Chapter-III

Surfactants assisted synthesis of CuAl-sodium dodecyl sulfate layered double hydroxide and its adsorptive removal of methyl red dye from aqueous solution

III.1. Introduction

Water pollution has become a global environmental problem due to the development of rapidly growing modern industry, increasing population, and climate change. The increased water pollution caused by various consumers have significantly contributed to and adversely intensified the contamination of scarce and fresh water resources.[1] Recently, the major water contaminants are organic azo dyes, which are utilized in various industries, including textile, paper, cosmetics, and food industries, for coloring and dyeing purposes.[2] Subsequently, a large amount of waste water is generated, which is directly drained over natural water bodies such as lakes, seas, oceans, rivers, etc. Since dyes are generally complex organic compounds and chemically inactive, they are synthesized to overcome degradation from various contacts like sunlight, water, and detergents.[3] Therefore, it is difficult to remove it easily and can influence the environment by creating short and long-term effects.[4] In addition, these organic pollutants, for instance, anionic methyl red dye, which contain –N=N- group in its structure, are responsible for various health issues, including respiratory tract damage, mucous membrane irritation, gastrointestinal disturbances, and liver damage, which pose a threat to the global environment.[5] The serious consequences like carcinogenicity and bio toxicity due to dye polluted effluents observed in aquatic plants and animals are also reported.[6] Hence, extraction of organic azo dye pollutants from waste water is very crucial.

In order to mitigate the problem, today's researchers have adopted various methods for removing azo-dye contaminants from effluent, which may include adsorption, filtration, photocatalytic degradation, magnetic separation, reverse osmosis, and flocculation.[7-12] Among different techniques employed, adsorption is one of the most efficient processes for treatment of toxic contaminant. Due to less expensive, more convenient and less generation of waste product, it is considered to be more appropriate compare to others techniques. Another advantage of this method relies on the reversible characteristics between adsorbate-adsorbent systems, which can facilitate ease regeneration of the adsorbent material for repeated usage. As a result, adsorption

can also be regarded as the most extensively used and promising method for developing nations.[13] Some of the previously reported materials applied for detoxification of aqueous media include metal organic framework, biogenic nanocomposite, activated carbon-nanocomposite, bentonite, biochar, and mixed metal oxides.[14,15] However, owing to the lower adsorption capacity and reusability of these sorbents, currently a large number of researchers are currently interested in the modification or fabrication of the material structure to increase the monolayer adsorption capacity and the effective elimination of dye sunstances from its aqueous media.

Layered double hydroxides are anionic clays generally constructed by the brucite-type layers, which comprises of divalent M^{2+} and trivalent M^{3+} cation along with intergallery anions like A^{2-} lying between the brucite layers. In addition, the high-density positively charges layer is balanced by the intergallery anions, and the metal cations are coordinated octahedrally by the hydroxyl group. In general, the molecular formula of LDH is represented by $[M_{1-x}^{2+}M_x^{3+}(OH)_2]^{X+}(A^{m-})_{x/m}.nH_2O$, where M^{2+} and M^{3+} are divalent and trivalent cations, and A is a counter anion with negative charge m.[16] Accounting to its unique nature, LDH is not only confined to the field of catalysis; rather, its ability to tune its heterostructure through isomorphic substitution, intercalation, and surface modification makes it versatile and has potential applications in miscellaneous fields, including catalysis, drug delivery, flame retardants, and environmental remediation's.[17,18] Concerning the highly efficient and multi-dye removal adsorbent, the search for a better synthetic protocol for altering the surface of LDH with organic surfactants is extensively under study. Usually, in the traditional methods of LDH synthesis, due to the presences of hydrated interlayer ions such as Cl^-, NO_3^-, and CO_3^{2-}, it imparts hydrophilic properties to the LDH particle. As a result, it does not preferentially adsorbed cationic dyes and non-ionic organic molecules.[19] Therefore, fabrication with organic sodium dodecyl sulphate molecules can provide a hydrophobic nature to the resultant LDH material, which is essential for the removal of hydrophobic organic dye pollutants from waste water. The surface alteration with surfactants in the previous work reported by Zhang et al. can significantly enhance the adsorption behavior of LDH during the removal of methyl orange dye.[20] All these modified LDHs have a broad range of applications in the environmental remediation field.

In this study, we have investigated the decontamination of dye-polluted water with surfactant-fabricated LDH and compared it with its parent, pristine LDH. The synthesized adsorbents CuAl-LDH and CuAl-SDS-LDH are characterized and used for investigating their adsorption performance for the removal of methyl red dye from aqueous solutions. Under the study, we have reported the effect of various physical parameters such as contact time, adsorbent dosages, pH, temperature, and reusability. From our literature study till now, no reports regarding the sorption of methyl red by LDH are available. However, the results shown by the present materials are impressive. The possible mechanisms involved in kinetics and isotherm studies during the reaction are also illustrated.

III.2. Experimental

III.2.1. Materials and Methods

The precursors materials are copper nitrate trihydrate ($Cu(NO_3)_2.3H_2O$), aluminium nitrate nonahydrate ($Al(NO_3)_3.9H_2O$), sodium hydroxide (NaOH), sodium dodecyl sulfate ($CH_3(CH_2)_{11}SO_4Na$, and methyl red ($C_{15}H_{15}N_3O_2$, M.W-269.3 g/mol). All the chemicals are of analytical grade, purchased from Merck India, and utilized for the synthesis of materials without any further purification. In addition, under all experimental conditions, the required solution was prepared by using distilled water.

III.2.2. Synthesis

The sample represented as CuAl-LDH was prepared by a simple co-precipitation method where the ratio of divalent and trivalent cations M^{2+}/M^{3+} was maintained at 2:1 with a slight modification from the previously reported literature. The first metal precursor solution A was obtained by mixing 0.2 M $Al(NO_3)_3.9H_2O$ and 0.4 M $Cu(NO_3)_2.3H_2O$ in an aqueous solution of 100 mL. The second solution B contains 0.2 M NaOH in 150 mL distilled water. Subsequently, solution B is then added slowly, drop-wise, to solution A up to 30 minutes under vigorous stirring at room temperature with simultaneous maintenance of pH at (9-10). Furthermore, the reaction mixture is allowed to stir continuously for 24 hours. The blue-color slurry is obtained, which is then centrifuge and washed with distilled water several times until the pH of the filtrate

is neutral. The resulting product was obtained by drying in an oven at 50 ℃ for 12 hours and being crushed with mortar to get powder form.

For the synthesis of surfactant assisted CuAl/SDS-LDH, similar procedures have been carried out, except 0.5 g of sodium dodecyl sulfate has been added to solution B, and the remaining steps are performed under identical conditions as similar to earlier pristine CuAl-LDH material.

III.2.3. Adsorption Experiment

The adsorption experiments were performed by adopting the batch equilibrium adsorption method under a constant temperature of 28 ℃. For the study of adsorption isotherm, a series of methyl red dye solutions containing a total volume of 20 mL each with different concentrations ranging from 25 mg/L to 350 mg/L was taken in a 150 mL conical glass bottle. Subsequently, 22 mg of the adsorbent was added to the dye solution, which was then allowed to shake in a thermostatic shaker machine for a time period of 6 hours to reach equilibrium adsorption. After completion of shaking, the solution was filtered, and the concentration of dye remaining in the filtrate was measured by using UV-spectrophotometer (EI-3315) at 432 nm. The amount of methyl red dye adsorbed on the adsorbent was evaluated by the formula:

$$q_e = \frac{(C_0 - C_e)\,V}{W} \qquad (3.1)$$

The percentage of dye uptake was evaluated as:

$$\%\ \text{of dye uptake} = \frac{(C_0 - C_e) \times 100}{C_0} \qquad (3.2)$$

where, C_e and C_0 are the equilibrium concentration and initial concentration of methyl red dye, respectively. V is the volume of the solutions in litres (L) and W is the weight of adsorbent used in grams (g).

In the adsorption kinetics experiment, 44 mg of the adsorbent was mixed with 50 mL of the methyl red dye solution, having initial concentration of 60 mg/L, and then the resulting solution was shaken. After a definite time interval, the solution was withdrawn from the conical flask, and

the residual dye concentration was measured. The variation in the amount of dye adsorbed at different time intervals was studied for a time period of up to 4 hours. The amount of dye adsorbed with time was calculated by the formula:

$$q_t = \frac{(C_0 - C_t)\,V}{W} \qquad (3.3)$$

where, C_0 and C_t are the initial concentration of dye solution and concentration at time t, respectively. q_t is the amount of dye adsorbed at time *t*. However, in order to obtain better reproducibility, all the experiments are carried out twice.

III.2.4. Characterization techniques

X-ray diffraction analysis was conducted with a Rigaku Ultima-IV powder X-ray diffractometer at a braggs angle ranging between 5-70° by employing CuKα (λ=1.54 Å) radiation. Fourier transform infrared spectroscopy (FTIR) was recorded on SHIMADZU-IR Affinity-1 at a frequency range of 300-4000 cm^{-1} by using KBr background. The microstructure morphology of sample was investigated by Gemini Carl Zeiss Sigma 300, and the elemental composition was studied by EDX. The thermal degradation of the sample was investigated at temperatures ranging from 29 to 900 ℃ by using TGA at a ramping rate of 20 ℃/min. The textural properties of the as-synthesized CuAl-LDH, including specific surface area, pore size, pore volume, were analyzed in an instrument Quantachrome Novawin version 11.05 by performing adsorption-desorption of the N_2 gas at 77.3 K. Initially, the sample was out gassed at 150 ℃ for 6 hours. The BET (Brunauer-Emmett- Teller) method was used for the evaluation of specific surface areas, whereas for pore size and pore volume, the BJH (Brunauer-Joyner-Hallenda) method was employed. The measurement of the concentration of the unknown dye solution was made in a UV-Spectrophotometer-3375 (Electronics India).

III.3. Results and Discussions

III.3.1. Characterization of adsorbents

The analysis of the structure and crystalline size of the adsorbent material was investigated with the help of the powder XRD technique. The measurement of crystallite size was performed by using the Debye-scherrer equation, $D = B\lambda/\beta_{1/2}\cos\theta$, where $\beta_{1/2}$ denotes full width at half maximum (FWHM), B indicates the scherrer constant, λ signifies the wavelength of the X-ray, and θ is the diffracted angle. The XRD diffraction pattern is presented in **Fig III.1**. The synthesized CuAl-LDH shows sharp reflections corresponding to indexed planes 003, 006, 009, 015, 018, 110, and 113, which infers the formation of well-crystallized layered structure with basal spacing of 7.4 Å (d_{003}). The lattice cell parameters evaluated from the positions of diffraction planes 110 ($a = 2d_{110}$) and 003 ($c = 3d_{003}$) are 0.03 nm and 2.22 nm, respectively. These values are consistent with the previously reported literature.[21] However, modification with surfactants in the LDH structure leads to shifting of the peaks at a lower angle, which results in increasing the interlayer distance of CuAl/SDS-LDH, and the theoretically calculated length of basal spacing was found to be 14 Å. The observed results suggest intercalation of the sodium dodecyl sulfate molecule in the interlamellar region as well as assemblage on the external surface of LDH. Accounting for LDH thickness (0.48 nm) and the length of SDS chain, which is taken as 1.78 nm, the possible alignment of SDS inside the layer sheets is tilted with respect to LDH sheets. The diffraction peaks of CuAl/SDS-LDH at a higher angle are quite similar to those of parent LDH, which indicates the retention of LDH structure, whereas the initially observed peaks corresponding to reflection plane 015, 018 vanish, which may be attributed to the lowering in the stacking order of LDH sheets.[22,23-24] Nevertheless, the appearance of 001 plane at $2\theta < 7$ from which the basal spacing value is evaluated is observed in most of the organo-modified LDH, which is obvious in the currently studied material.

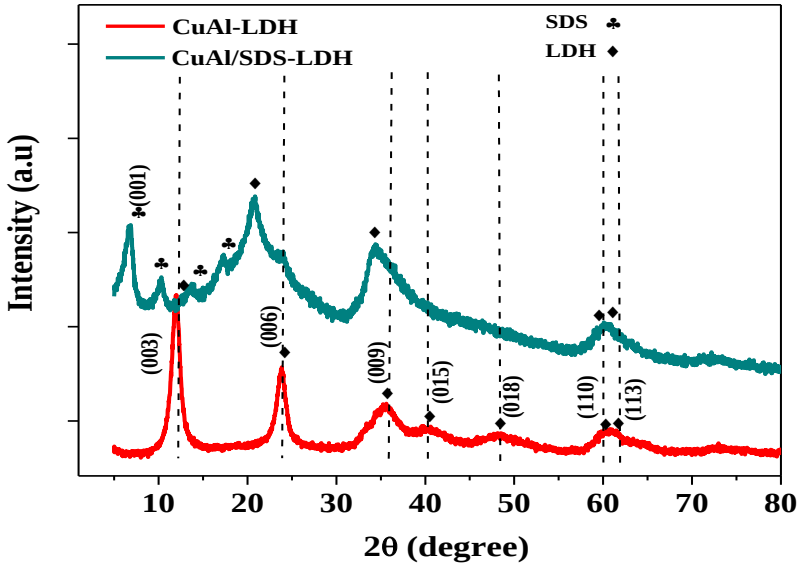

Fig III.1: XRD patterns of pristine CuAl-LDH and surfactants modified CuAl/SDS-LDH.

The FTIR spectrum of CuAl-LDH, CuAl/SDS-LDH before and after the adsorption of methyl red dye is displayed in the **Fig III.2**. In CuAl-LDH, the observed bands are highlighted at the stretching frequencies of 3447 cm^{-1}, 1626 cm^{-1}, 1383 cm^{-1}, 827 cm^{-1}, and 639 cm^{-1}. The broad band at 3447 cm^{-1} indicates the presence of interlayer water molecules corresponding to the υ-OH stretch of free and H-bonded OH groups. The broadness of such a band increase with the number of increasing H-bonding, which could be possible among interlayer NO_3^-, H_2O, and OH^- ions. Another absorption at 1626 cm^{-1} is due to O-H bending vibration of water molecule present in the interlayer region of LDH. Furthermore, the presence of NO_3^- is also revealed at 1383 cm^{-1} and 827 cm^{-1}, which are assigned to anti-symmetric stretching mode and non-planar bending mode vibration respectively. And the less intense band at 639 cm^{-1} can be attributed to the M-OH stretching vibration.[21,25] After modification with the surfactant molecules the bands manifested at 2851 cm^{-1}, 2920 cm^{-1}, 1066 cm^{-1}, and 811 cm^{-1} can be related to δ-CH_2 symmetric stretch, δ-CH_2 asymmetric stretch, S-O-C bond stretch, and out of plane SO_3^{2-} stretch, respectively.[20]

The new additional weak and sharp band at 1417 cm^{-1} and 1359 cm^{-1} arises in CuAl/SDS-LDH after incorporation of methyl red, which corresponds to -CH_3 deformation and the C-N stretching vibration of the dye molecule. The appearance of a weak band at 1417 cm^{-1} and 1104 cm^{-1} in CuAl-LDH after adsorption also accounts for –CH_3 deformation and C-H in the plane bending vibration of the adsorbate. The obtained results confirm the presence of the target dye pollutant on both adsorbents.[26]

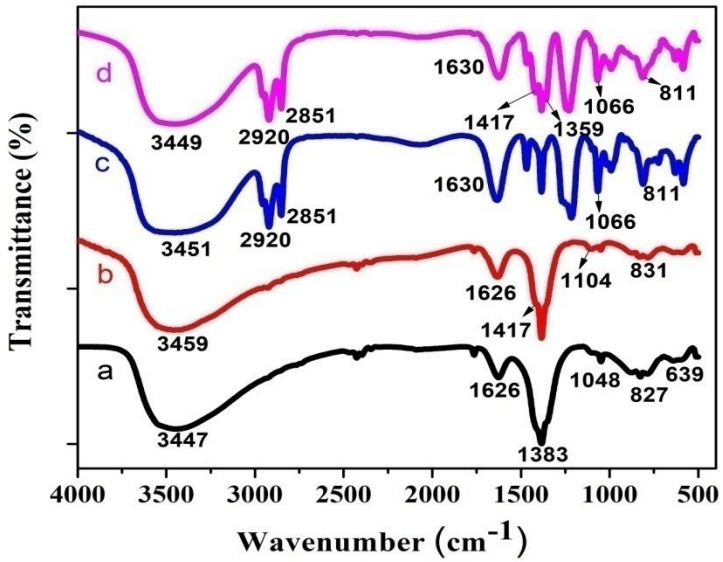

Fig III.2: FTIR spectrum before and after adsorption of methyl red dye (a) CuAl-LDH (b) CuAl-LDH-methyl red (c) CuAl/SDS-LDH (d) CuAl/SDS-LDH-methyl red.

To illustrate the surface characteristics, the N_2 adsorption-desorption isotherm and pore size distribution curves of the adsorbent are presented in **Fig III.3(a, b)**, respectively. The specific surface areas of CuAl-LDH and CuAl/SDS-LDH were determined to be 65.146 and 74.055 m^2/g, respectively. The presence of mesopores (9.086 nm) in the distribution can be anticipated from the analysis, which is shown in the insets of **Fig III.3(a, b)**. In addition to the N_2 adsorption-desorption curves of both materials, it manifests type IV isotherm with H3 hysteresis loop, which is according to the IUPAC classification and signifies mesoporous materials.[27,28] Moreover, the measured pore volumes of CuAl-LDH and CuAl/SDS-LDH are 0.289 cc/g and 0.178 cc/g, respectively. After introduction of surfactant, it is apparent that the relatively higher surface area

and mesoporous characteristics of CuAl/SDS-LDH provides it with larger adsorption site and makes it more suitable for adsorption performance of this materials**.**

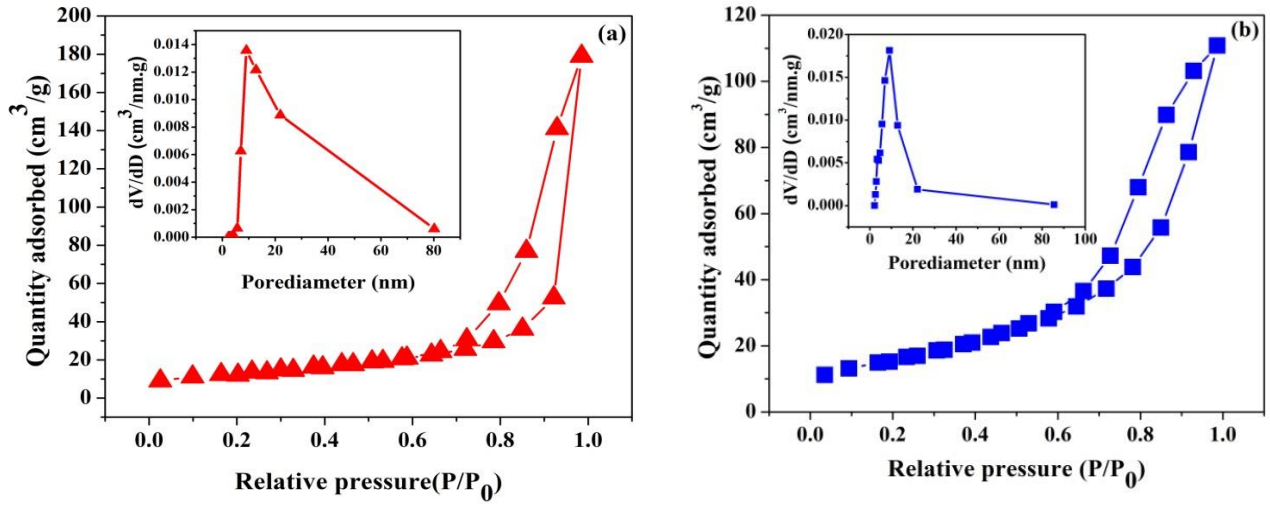

Fig III.3: N_2 adsorption-desorption isotherm and pore size distribution of (a) CuAl-LDH and (b) CuAl/SDS-LDH.

The thermal stability of the synthesized CuAl–LDH and CuAl/SDS-LDH were studied by thermogravimetric analysis which is displayed in **Fig III.4(a, b).** From the TGA curve of CuAl-LDH two distinct region of weight loss can be identified. The mass loss of 9.67% noticed at temperature below 210 ℃ can be ascribed to the evaporation of adsorbed water molecules while the weight loss of 28.16% between 230-450 ℃ is due to the removal of intergallery ions and hydroxyl group of the LDH sheets.[29,30] In contrast, the CuAl/SDS-LDH showed the weight loss of 9.11%, 32.31% and 19.64% at three different stages. The weight loss of 9.11% corresponding to first step is similarly related to the removal of physical surface adsorbed water molecules. The major amount of 32.31% weight loss has been observed between the temperature 165-260 ℃ which is associated with the decomposition of surfactants molecule embedded on LDH. In addition the final step of mass decomposition can be accounted for the elimination of intercalated inorganic anions and breakdown of LDH sheets.[31] For CuAl-LDH after the decomposition at the

temperature of 435 ℃, the curve tends to be constantly straight which indicates no further weight loss whereas in CuAl/SDS-LDH it was achieved after 580 ℃ and the complete destruction of material structure is obtained beyond this temperature.

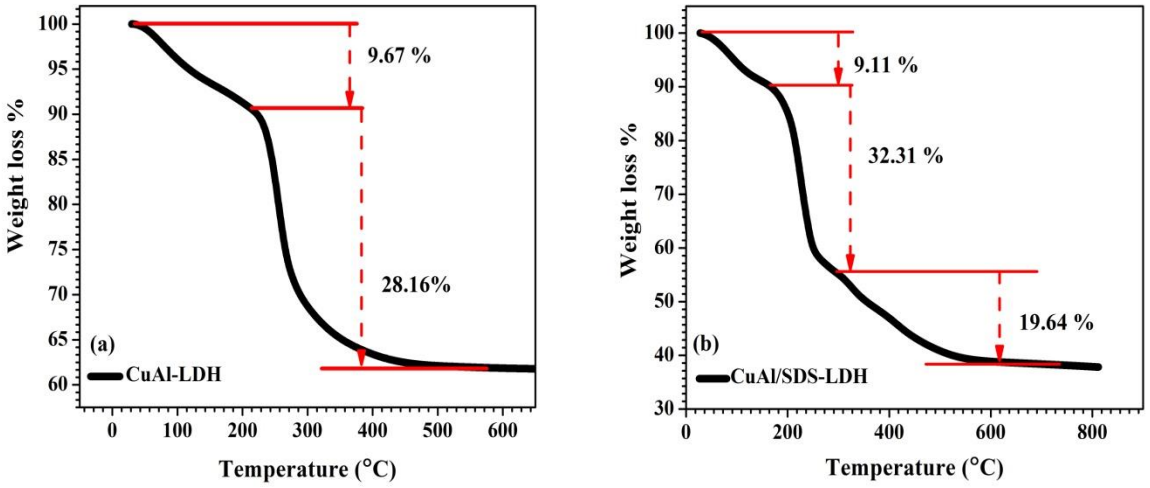

Fig III.4: TGA curves of (a) CuAl-LDH and (b) CuAl/SDS-LDH.

The FE-SEM micrographs pattern of CuAl-LDH and CuAl/SDS-LDH are depicted in **Fig III.5(A-D)**. The study of surface morphology shows formation of porous and thin sharp sheet like structure having a dimension below 100 nm in CuAl-LDH, which may be attributed to the irregular and non uniform arrangement of layer structures. It is also evident from the image **Fig III.5(A)** that the LDH particles are highly dispersed and found stacked with each other. After fabrication with surfactants the FE-SEM image of CuAl/SDS-LDH illustrates reduction in sharpness of LDH sheets and the growth in thickness of particle size due to expansion of interlayer region.[21,32]

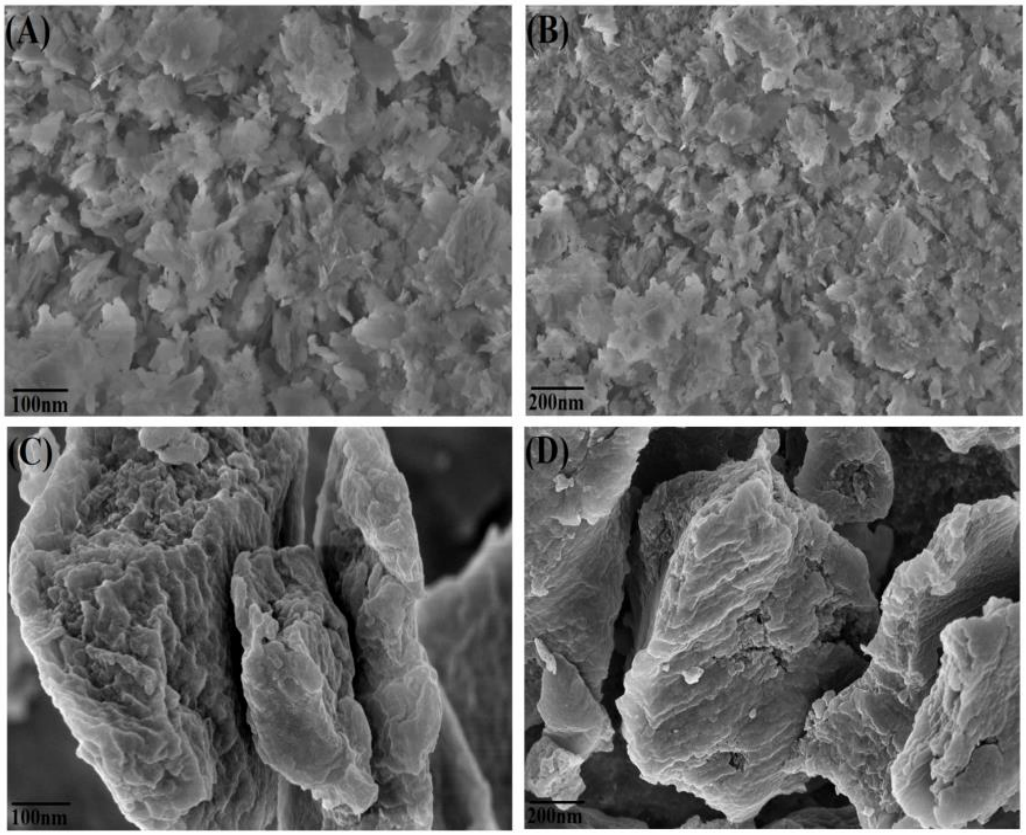

Fig III.5: FE-SEM images of CuAl-LDH (A, B) and CuAl/SDS-LDH (C, D).

The elemental analysis spectrum of the CuAl-LDH and CuAl/SDS-LDH is presented in **Fig**. **III.6(A, B).** The chemical constituents of the synthesized LDH were determined by energy dispersive x-ray method which indicates the formation of LDH with expected molar ratio of Cu^{2+}/Al^{3+} (2:1) close to 2 as shown in **Table III.1**. The observed atomic percentage of the elements Cu, Al and O are 18.23 %, 10.71 % and 71 %, respectively. Similarly, the EDX spectrum of CuAl/SDS-LDH also confirms the presences of all the constituent elements. Moreover, the presences of other impurity elements of the precursor solutions like alkali metals are not detected thereby confirming efficient synthetic procedure and resulting in to pure form of sample.

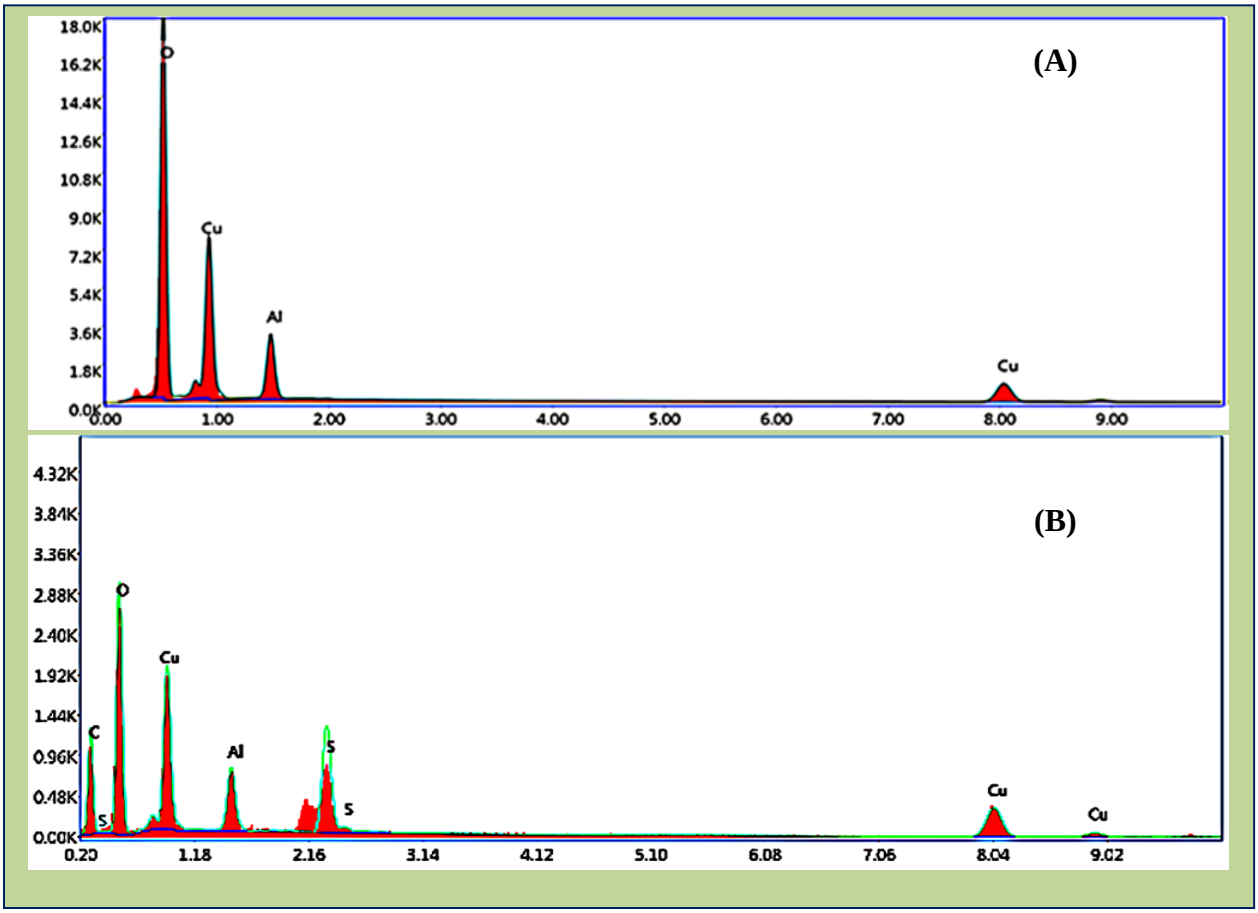

Fig III.6: (A) EDX spectra of CuAl-LDH **(B)** EDX spectra of CuAl/SDS-LDH.

Table III.1: Atomic percentage of the constituent elements present in the proposed adsorbent determined by EDX analysis**.**

Adsorbents	Cu %	Al %	C %	O %	S %
CuAl-LDH	18.23	10.76	-	71	-
CuAl/SDS-LDH	6.87	3.35	42.77	42.78	4.24

SDS = Sodium dodecyl sulfate, LDH = Layered Double Hydroxide, EDX = Energy Dispersive X-ray

III.3.2. Adsorption Isotherm

In order to have detailed information considering the affinity of targeted anionic dyes towards the proposed adsorbent materials, the distribution of dye molecules between the solid and liquid phases after reaching the equilibrium stage can be best understood from the study of the adsorption isotherm. With the help of isotherm studies, it is also possible to interpret the qualitative nature of the adsorbate-adsorbent system. For a clear illustration of the adsorption behavior and its underlying mechanisms, three models, including Langmuir, Freundlich, and Temkin, are employed. These model isotherms can easily explain the relationship between the quantity of dye adsorbed and the equilibrium concentration.[33]

III.3.2.1. Langmuir Isotherm

It is a monolayer adsorption model that assumes that if the complete saturation of the homogeneous vacant site of the adsorbent surface is reached, then there is no further additional occupation of those sites by the adsorbate molecules.[34] The non-linear form of Langmuir equation is represented as:

$$q_e = \frac{q_m C_e K_l}{1+K_l C_e} \qquad (3.4)$$

where, q_m, C_e , q_e, and K_l represents highest monolayer adsorption capacity, final equilibrium concentration of dye solution (mg/g), quantity of dye adsorbed at equilibrium (mg/L), and Langmuir constant, respectively.

Fig III.7(a-d) shows different isotherm model plots for the removal of methyl red dye. With the help of the Langmuir isotherm plot, the highest monolayer adsorption capacity q_{max} value for the adsorbents CuAl/SDS-LDH (411.47 mg/g) and CuAl-LDH (209.97 mg/g) was evaluated. The favorability of the adsorption process was determined by a factor R_L, which is calculated from the equation:

$$R_L = \frac{1}{1+K_l C_0} \qquad (3.5)$$

where C_0 and K_l are the initial dye concentration and Langmuir constant, respectively. Moreover, if the equilibrium parameter R_L >1, then the adsorption process is unfavorable, and for values of R_L between 0 and 1, it indicates a favorable process, while for an irreversible process, R_L= 0. The obtained results shown in **Fig III.8(a, b)** indicate that for both adsorbents at different initial dye concentration, R_L values lie in the range from 0 to 1, which infers the feasibility of the adsorption process.[35]

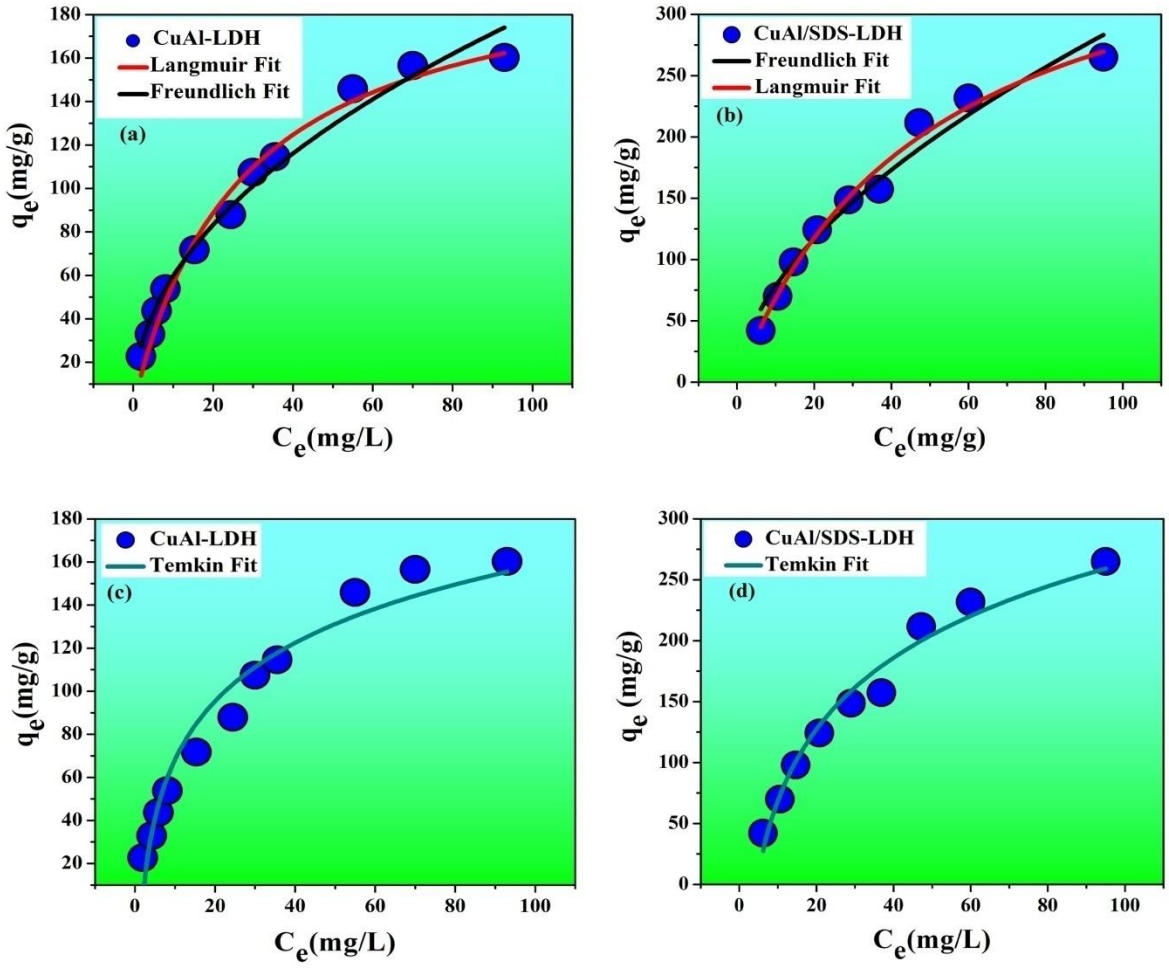

Fig III.7: Non linear plot of adsorption isotherm by using Langmuir, Freundlich and Temkin model for adsorption of methyl red dye on CuAl-LDH (a, c) and CuAl/SDS-LDH (b, d).

III.3.2.2. Freundlich Isotherm

The Freundlich isotherm is an empirical equation representing the relationship between quantities of solute adsorbed per unit mass of solid adsorbent. This model is more suitable for studying the adsorption on the heterogeneous surface of the adsorbent.[36] The equation for Freundlich isotherm is given as:

$$q_e = K_f C_e^{1/n} \qquad (3.6)$$

where, q_e and C_e have their usual meaning and K_f and n are constants that provide information regarding capacity and intensity of adsorption, respectively.

III.3.2.3. Temkin Isotherm

Concerning the interaction between the adsorbate-adsorbent system, Temkin isotherms considers that the heat of adsorption of all the molecules present on the surface of LDH sheets get reduced linearly with surface coverage. And the nature of the adsorption is best described by the orderly arrangement of binding energies until a certain maximum value.[37] The non-linear equation of the Temkin isotherm is given as:

$$q_e = B_T \ln (K_T C_e) \qquad (3.7)$$

where, B_T (KJ/mol) and K_T (L/mg) signify the heat of adsorption and equilibrium binding constant, respectively.

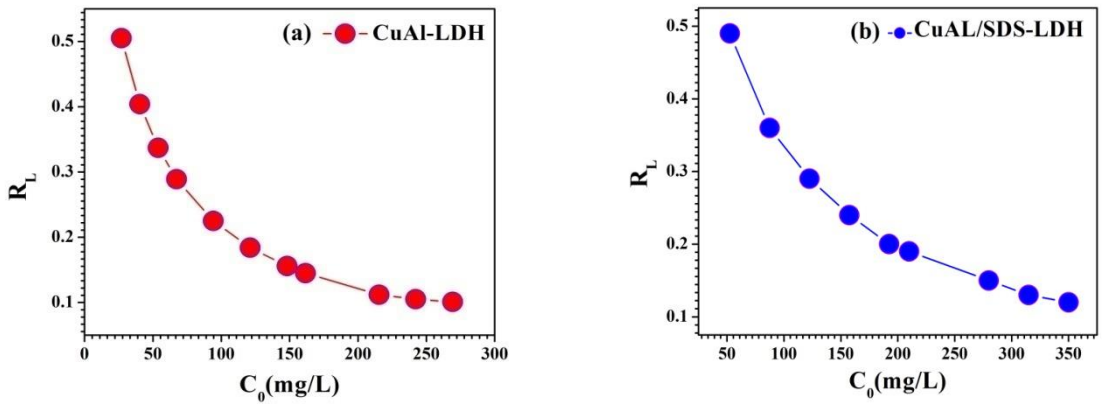

Fig III.8: Plot of R_L vs C_0 for adsorption of methyl red dye over two adsorbents (a) CuAl-LDH and (b) CuAl/SDS-LDH

The various adsorption isotherm parameters are summarized in **Table III.2.** The observed results from the adsorption isotherm data after non-linear fitting showed a greater coefficient of determination R^2 value for Langmuir fitting in comparison to Freundlich and Temkin fitting, which implies that the Langmuir model can best account for the adsorption mechanism. Consequently, the surfaces of the applied adsorbent are closer to homogeneous than heterogeneous. The K_f values for CuAl-SDS LDH and CuAl-LDH were determined to be 21.18 and 19.74, respectively. In addition, the values of constant *n* greater than 1 in both adsorbents suggest that the adsorbate gets suitably adsorbed on the material surface under the studied experimental conditions.

Table III.2: Isotherm parameters for adsorption of methyl red onto CuAl-LDH and CuAl/SDS-LDH

		Adsorbents	
Isotherm model	**Constants**	**CuAl-LDH**	**CuAl/SDS-LDH**
Langmuir	K_l (L/mg)	0.0365 ± 0.004	0.0200 ± 0.002
	q_{max} (mg/g)	209.97 ± 11.46	411.47 ± 15.22
	R^2	0.981	0.985
Freundlich	*n*	2.0825 ± 0.12	1.756 ± 0.14
	K_f	19.744 ± 2.17	21.180 ± 3.90
	R^2	0.978	0.961
Temkin	B_T	39.088 ± 2.82	84.635 ± 5.15
	K_T	0.5733 ± 0.10	0.2249 ± 0.02
	R^2	0.950	0.971

Experimental Conditions: Initial Conc. (C_0) = 25-350 mg/L, dosage = 22 mg, temperature = 28 ℃, time = 6 hours

In order to assess the adsorption performance of the currently proposed LDH, it is compared with the previously reported material, which is displayed in **Table III.3.** It highlights the maximum adsorption capacity and optimum experimental conditions of several adsorbents for the elimination of methyl red dye from an aqueous medium. It is clear from **Table III.3** that the dye adsorption capacity of the proposed LDH material is comparatively higher than some of the

adsorbents such as biogenic Ag@Fe nanocomposite, MIL-53(Fe), and Pd-NP-AC, while other adsorbents showed greater monolayer adsorption capacity. However, few of these materials involve harsh and complicated synthetic methods. In contrast, the synthesis of pristine and surfactant LDH involves simple and less toxic reactions, which is an advantage of the present materials. Therefore, it can be concluded that CuAL-LDH and CuAl/SDS-LDH can be considered promising materials for the removal of methyl red dye in terms of their less toxic, low cost, and good adsorption performances.

Table III.3: Comparison of various adsorbents used for removal of methyl red dye**.**

Adsorbents	q_{max} (mg/g)	pH	Time (min)	Dosages (g)	Isotherm	Ref.
Biogenic Ag@Fe nonocomposite	125	5	160	0.042	L	14
Natural raw Clay Anb	397	7	5	0.25	L	38
Pd-NP-AC activated carbon	133.33	2	15	0.01	L	39
Fe_3O_4@MIL-100(Fe)	625	4	360	0.01	L	40
Custard apple derived activated carbon AC	434.78	5	50	0.15	L	41
Durian seed derived activated carbon AC	384.62	6	180	0.10	L	42
MIL-53(Fe)	183.5	4	120	0.05	L	43
CuAl-LDH	209.97	7	360	0.022	L	This work
CuAl/SDS-LDH	411.47	7	360	0.022	L	This work

Maximum monolayer adsorption capacity = q_{max} (mg/g), L = Langmuir isotherm, AC = activated carbon, SDS = Sodium dodecyl sulfate, NP = Nanoparticle, MIL = Materiaux de I′ Institut Lavoisier

III.3.3 Adsorption Kinetics

The evaluation of various kinetic parameters can have essential practical value for technological utilization. In the present study, in order to estimate the rate of dye adsorption and to have the detailed information about the regulated mechanism, a kinetic study was performed, and the two

different most widely used kinetic models, namely pseudo-first order and pseudo-second order, were adopted for the determination of kinetic parameters. Based on the physical adsorption pseudo–first-order kinetic model, it is considered that the rate of dye intake is proportionate to the ratio of the concentration of dye and the quantity of adsorbent used. On the contrary, pseudo-second-order kinetics depends on chemisorptions, where the chemical bond, either covalent or ionic, holds the adsorbate-adsorbent system.[44,45] The linear form of the pseudo-first-order, pseudo-second-order kinetic, and intraparticle diffusion equation is formulated as

$$\log (q_e - q_t) = \log q_e - \frac{K_1\, t}{2.303} \quad (3.8)$$

$$\frac{t}{q_t} = \frac{1}{K_2 q_e^2} + \frac{t}{q_e} \quad (3.9)$$

$$q_t = K_i\, t^{0.5} + C \quad (3.10)$$

where, q_e and q_t represents the quantity of adsorbate taken up by an adsorbent under equilibrium and time *t* (min), respectively. As shown in **Fig III.9(a)**, the linear plot of log ($q_e - q_t$) vs *t* gives a straight line from which the obtained slope and intercept values are used in the determination of the first-order rate constant $K_1$and q_{e1} amount of dye adsorbed at equilibrium, respectively. Nevertheless, from the **Fig III.9(b)**, the plot of (t/q_t vs *t*) evaluates the pseudo-second-order rate constant K_2 and the quantity of dye adsorbed at equilibrium q_{e2}.

The detailed kinetic parameters are depicted in **Table III.4**. From the obtained results, it can be anticipated that the experimental data fits well with the pseudo-second-order kinetic model, with greater coefficient of determination (R^2 >0.994) value in comparison to the first-order kinetic model. Moreover, it is also evident that the pseudo-second-order rate constants for CuAl-LDH and CuAl/SDS-LDH are 5.77×10^{-4} g.mg^{-1}min^{-1} and 4.29×10^{-4} g.mg^{-1}min^{-1}, respectively, which implies that the sorption rate of methyl red dye on CuAl-LDH is faster than CuAl/SDS-LDH. Besides, the higher experimental $q_e$value for CuAl-SDS (69.48 mgg^{-1}) compare to CuAl-LDH (37.44 mgg^{-1}) further conveys enhancement in adsorption capacity of surfactants assisted LDH. In the adsorption process of methyl red dye, the relatively closer values of pseudo-second order q_{e2} with q_e in both the adsorbent infer that during the studied experimental conditions for

initial dye concentration of 50 mg/L, and a contact time from 0-220 minutes, the adsorption behavior can be best described by pseudo-second-order mechanism. In addition, the values of calculated q_{e1} from pseudo-first-order in both adsorbents do not agree with experimental q_e. Thus, it confirms that the rate-determining step in the adsorption process may be due to chemisorption.

The mechanism of the diffusion process during the adsorption of methyl red dye has been described by employing an intraparticle diffusion model (equa.3.10). From **Fig III.9(c)**, the plot of q_t vs $t^{0.5}$ clearly manifests the appearance of multiple-step process in both the adsorption systems. The initial region observed in **Fig III.9(c)** indicates sorption on the external surface of the adsorbents, while the middle region represents occupation of dye molecules inside the pores, and the third region implies completion of the equilibrium stage of adsorption due to lack of available vacant sites.[46] The value of intraparticle diffusion constants K_i and the thickness of the boundary layer C was determined from the slope and intercept of the linear plot q_t vs $t^{0.5}$, which are demonstrated in **Table III.4**.

Table III.4: Parameters of three kinetic models for adsorption of 60 mg/L of methyl red by CuAl-LDH and CuAl/SDS-LDH.

Kinetic model	Parameters	CuAl-LDH	CuAl/SDS-LDH
	q_e (exp) mgg^{-1}	37.44	69.48
Pseudo-first-order	q_{e1} (cal)	45.90	46.08
	K_1 (10^{-3}) min^{-1}	22.36	16.65
	Δq	0.0714	0.1065
	R^2	0.90	0.96
Pseudo-second-order	q_{e2} (cal)	43.95	78.74
	K_2 (10^{-4}) $g.mg^{-1}.min^{-1}$	5.77	4.29
	Δq	0.0549	0.0421
	R^2	0.99	0.99
Intraparticle diffusion	K_i	2.28	4.05
	C	6.92	17.08
	R^2	0.95	0.84

Initial Concentration (C_0) = 60 mg/L, dosages = 44 mg, volume = 50 mL, time = 4 h, Dye = Methyl red

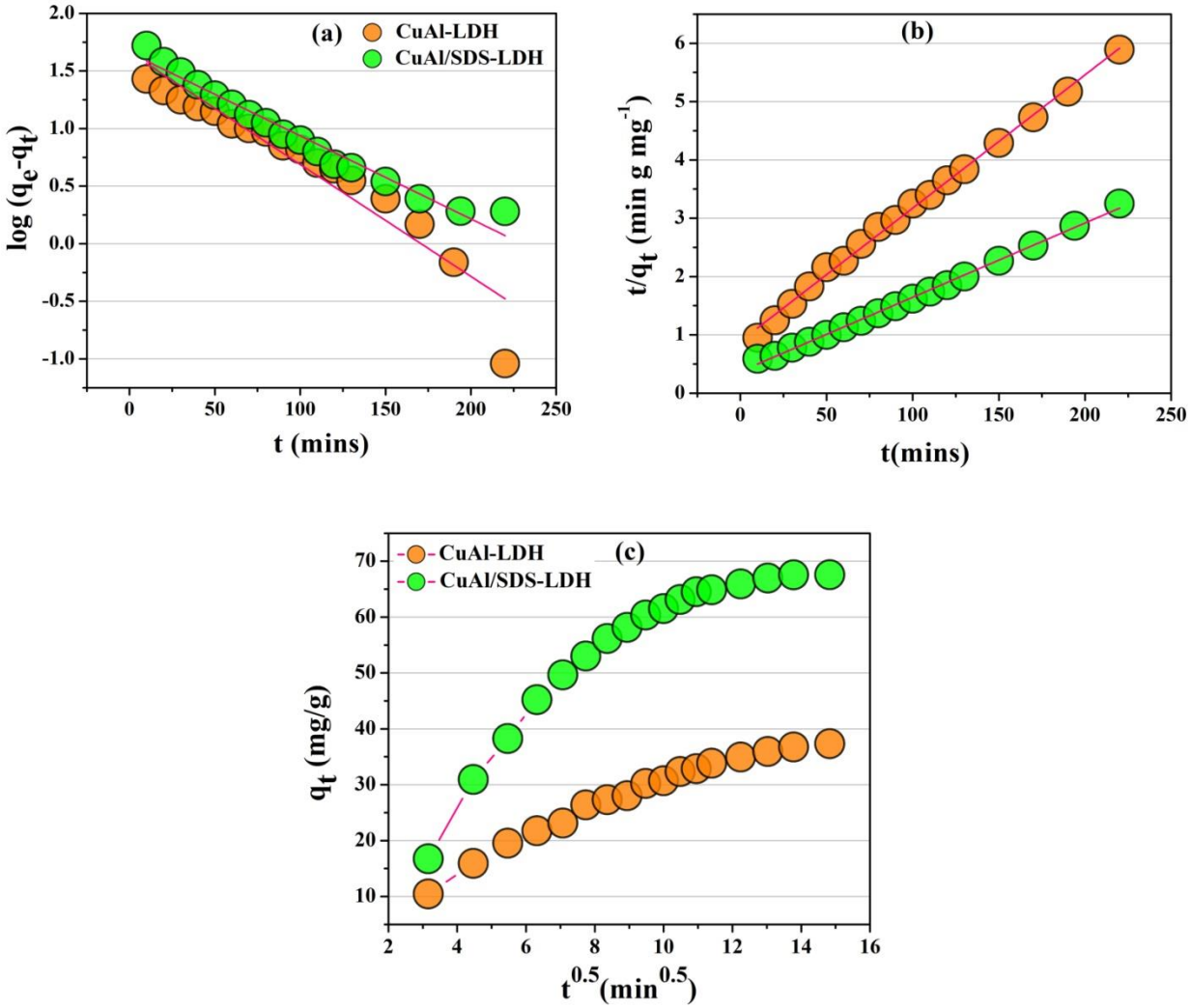

Fig III.9: (a) Pseudo-first-order kinetic plot for adsorption of methyl red on CuAl-LDH and CuAl/SDS-LDH. (b) Pseudo-second-order kinetic plot (c) Intraparticle diffusion kinetics plot.

III.3.3.1 Effect of temperature

Temperature is another important parameter affecting the adsorption of organic dye molecules on the surface of substrate, or LDH. In order to have a broad insight into the adsorption process with the change in temperature, the various parameters ΔG, ΔH, and ΔS were evaluated. The experimental reactions with varying temperature at 301 K, 313 K, and 323 K were performed on

90 mg/L of methyl red with 0.0220 g catalyst dosages for a contact time of 1 hour. The equations for the calculation of the thermodynamic parameters are given as:

$$\ln K_d = \frac{\Delta S}{R} - \frac{\Delta H}{RT} \quad (3.11)$$

$$\Delta G = -RT \ln K_d \quad (3.12)$$

where, ΔG, K_d, R, and T indicate standard free energy, adsorption distribution co-efficient, universal gas constant, and temperature (K), respectively.[47]

Table III.5. Thermodynamic parameters for adsorption of the methyl red on CuAl-LDH and CuAl/SDS-LDH.

Adsorbent	+ΔH(KJ/mol)	+ΔS(J/mol)	-ΔG(KJ/mol)		
			301 K	313 K	323 K
CuAl-LDH	9.11	34.16	1.12	1.58	1.94
CuAl/SDS-LDH	20.86	80.55	3.26	4.39	5.18

C_0 = 90 mg/L, dosages = 22 mg, temperature = 301 K, 303 K, 313 K, time= 1 h, volume = 20 mL, ΔG = Gibbs free energy (KJ/mol), ΔH = Enthalpy (KJ/mol), ΔS = Entropy (J/mol)

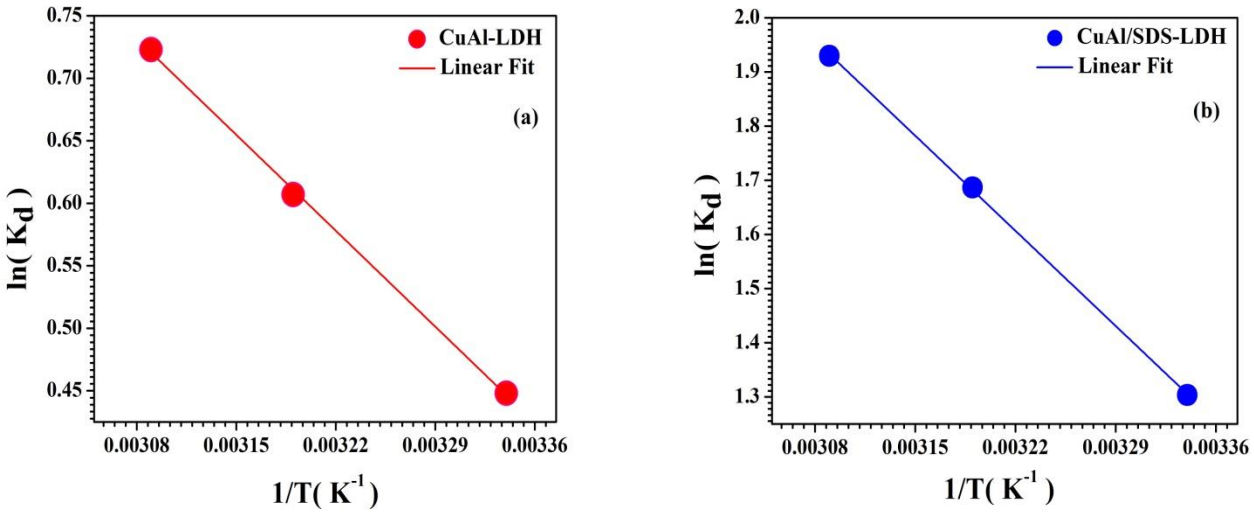

Fig III.10: Vant-Hoff plot for the adsorption behavior of the methyl red by the adsorbents (a) CuAl-LDH (b) CuAl/SDS-LDH. (Initial dye concentration = 90 mg/L, dosages = 22 mg, volume = 20 mL, contact time = 1 hour).

From the Vant-Hoff plot (ln K_d vs 1/T) shown in **Fig III.10(a, b)**, the values of enthalpy ΔH and entropy ΔS are determined from the slope (ΔH/R) and intercept (ΔS/R), respectively. The results obtained from the thermodynamic parameters represented in **Table III.5** revealed the negative value of ΔG in both materials, CuAl-LDH and CuAl/SDS-LDH, which infers the feasibility of adsorption process. With increasing temperature from 301 K to 323 K, ΔG value decreases from -1.12 to -1.94 KJ/mol (CuAl-LDH) and -3.26 to -5.18 KJ/mol (CuAl/SDS-LDH). The value of enthalpy change ΔH provides information to interpret if the nature of dye intake in the adsorption system is either physical or chemical. Moreover, values of ΔH lying between (-20 to 40) KJ/mole indicate physical nature of adsorption, whereas the value within (-400 to -80) KJ/mol refers to chemical nature. The positive values of ΔH and ΔS correspond to the endothermic and spontaneity of the process. The obtained ΔH values for CuAl-LDH and CuAl/SDS-LDH are +9.11 KJ/mol and +20.86 KJ/mol, respectively, which indicates physical nature of the process. Again, the entropy change ΔS value signifies the randomness of molecules in the solid-liquid interfaces.[48] However, there is a slight enhancement in the adsorption process with increasing temperatures in both adsorbents, thereby revealing that the adsorption process takes place through endothermic reactions. The obtained result shows that surfactant-assisted CuAl-LDH has greater adsorption for methyl red dye compared to pristine CuAl-LDH, which is achieved at a higher temperature 323 K. Initially, the positively charged external surface and intergallery region of the materials are saturated with dye molecules due to coulombic force and other interactions, possibly H-bonding and vander Waals. After filling up external surfaces, the dye molecule then gets attached to surfactant-loaded LDH via weak interactions.[20] From the experimental data, it suggests that surfactants can improve the capacity of dye removal. Therefore, CuAl-LDH and CuAl/SDS-LDH prove to be promising and effective adsorbents for the removal of anionic dyes.

III.3.3.2. Effect of initial dye concentration

The effect of initial dye concentration on the adsorption efficiency is depicted in **Fig III.11(a, b).** The removal efficiency of methyl red dye over CuAl-LDH and CuAl/SDS-LDH decreased with increasing initial dye concentration. It can be attributed to the less number of free sorption site on the adsorbent surfaces. Moreover, the type of adsorption process becomes monolayer at initial low concentration, which then further extends to multilayer after the complete saturation level is

achieved at the higher concentration of methyl red solution. As expected, it is not surprising that the time required to attained equilibrium is less at low initial concentrations, which is relatively higher in case of high initial concentrations. Nevertheless, in some cases, a higher dye concentration can increase the adsorption percentage due to the creation of a pressure gradient by a large number of dyes molecules on the adsorption site.[49] For the initial dye concentration of methyl red (25-120 mg/L) for CuAl-LDH, and (52-210 mg/L) for CuAl/SDS-LDH, the sorption percentage lies in the range of (79.81-92.79 %) and (82.45-88.30 %), respectively.

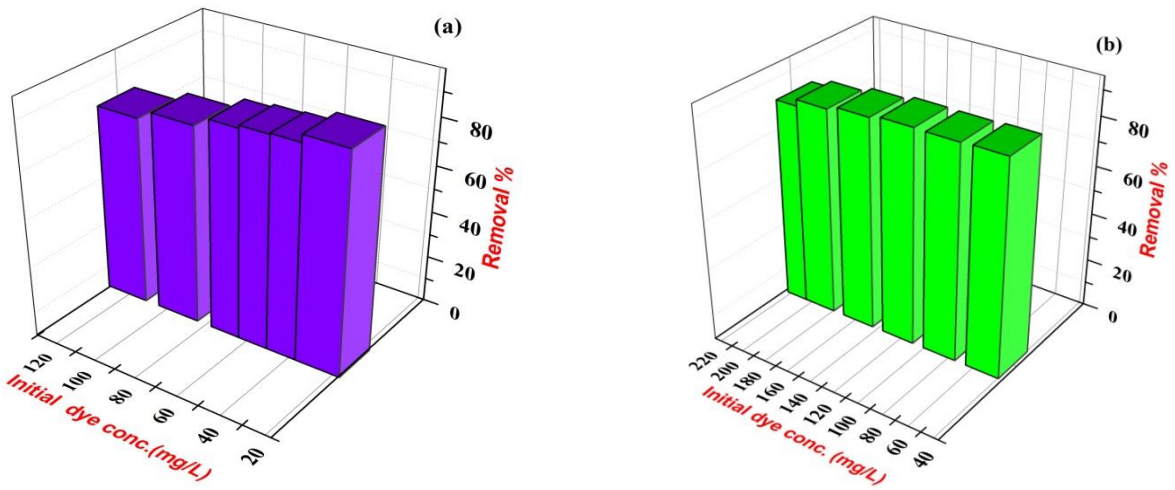

Fig III.11: Effect of the initial dye concentration on adsorption efficiency of methyl red over (a) CuAl-LDH and (b) CuAl/SDS-LDH. (Adsorbent dosages = 22 mg, volume = 20 mL, contact time = 6 hours)

III.3.3.3. Effect of Adsorbent dosages

It is very crucial to determine the suitable adsorbent dosages for the maintenance of cost-effective system. Subsequently, the variation in adsorbent dosages having a significant effect on the decontamination of methyl red dye from its aqueous solution was analyzed. From the **Fig III.12(a, b)**, the adsorption performance of SDS-modified CuAl-LDH at different dosages from 0.010 to 0.030 g is clearly distinguishable in comparison to that of pristine CuAl-LDH. However, with increasing adsorbent amount, the percentage of dye removal also increases in both material, but the surfactants modified LDH showed a relatively higher adsorption behavior. The observed

result implies that CuAl/SDS-LDH provide stronger electrostatic attraction and hold the target dye molecule more tightly. In contrast, the low positive charge on CuAl-LDH and lesser anion exchange capacity can account for the poor removal efficiency of methyl red. The amount of adsorbed dye increases sharply until 0.025 g, after this dose, the percentage of adsorption almost remains same. This could be attributed to the well-dispersed particle of the adsorbent material on the dye solutions where the active adsorption and interchangeable sites present over the surface of the adsorbent are more exposed.[20,50] Besides, the continuous and excessive increase in the amount of adsorbent can possibly cause the accumulation of LDH particles, which reduces the easily accessible adsorption site by lowering the specific surface area and providing a higher diffusion path length value.[51] Moreover, under the studied catalyst dosages the maximum percentage of dye removal was achieved up to 92 % and 42.24 % on CuAl/SDS-LDH and CuAl-LDH, respectively, for the initial dye concentration of 95 mg/L and a contact time of 1 hour at room temperature. The large number of available adsorption sites, increased catalyst amount, and high surface area can be responsible for the higher removal of dye.

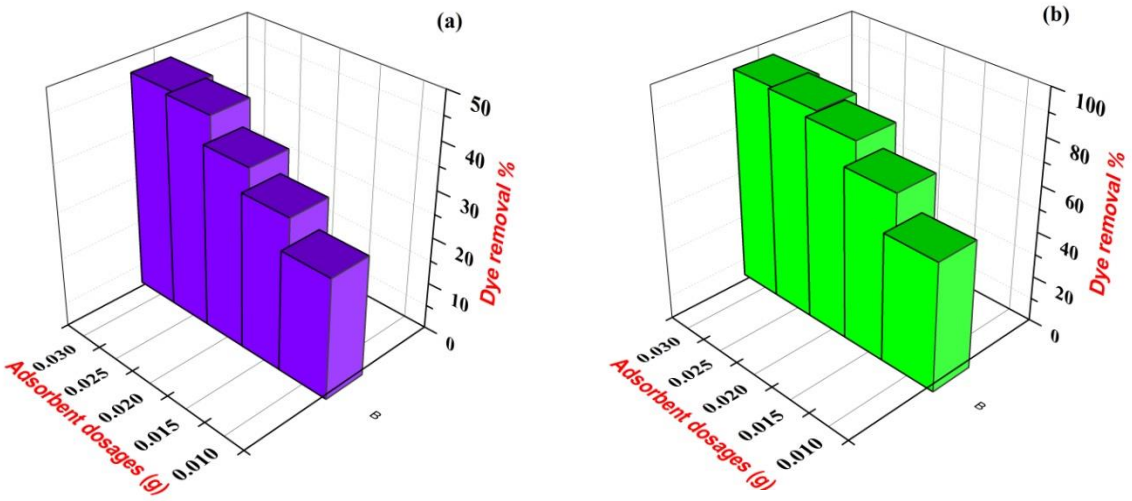

Fig III.12: Influence of adsorbent dosages on the removal efficiency of methyl red dye by CuAl-LDH (a) and CuAl/SDS-LDH (b) (Initial dye concentration = 95 mg/L, pH= neutral, contact time = 1 hr, volume = 20 mL)

III.3.3.4. Effect of contact time

With an emphasis on the rate of decontamination of dye from its aqueous solution, the contact time between the adsorbent and adsorbate molecules is an important factor. In general, most of the previously utilized LDH-based adsorbent, it has been observed that at the initial stage of contact time, the rate of dye removal is fast, which then gradually declines to a minimum and reaches the equilibrium stage. It is due to the sufficient and excess number of free available adsorption sites and the highest concentration gradient of adsorbate molecule at the initial stage.[52] The effect of contact time on the adsorbate-adsorbent system is represented in **Fig III.13**. It is evident that the rate of adsorption starts increasing rapidly after a contact time of 15 minutes. The rapid intake of dye molecules can be attributed to the presence of a large number of available vacant sites. However, during the adsorption process, the external surface and intergallery space of LDH are occupied by the dye molecules, with the association of different possible interactions, including electrostatic and H-bonding.[53] In CuAl-LDH, the curve displays inflexion at a contact time of 50-75 minutes, which can be ascertained due to the transportation of adsorbed methyl red molecules present on the external surface to the internal pores of LDH via slow diffusion. Consequently, the rate of adsorption started to decline.[54] The complete saturation of free vacant sites was attained at contact times of 120 and 150 minutes for CuAl/SDS-LDH and CuAl-LDH, respectively. Furthermore, it is also clear that for a similar initial concentration of methyl red dye, the removal capacity of SDS-modified LDH is found to be comparatively higher than that of CuAl-LDH. After complete saturation, there is a steric repulsion between incoming dye molecules and adsorbed dye molecules, which forms clusters with SDS loaded LDH. As a result, after reaching equilibrium contact time, the amount of dye adsorbed remains constant throughout the time.

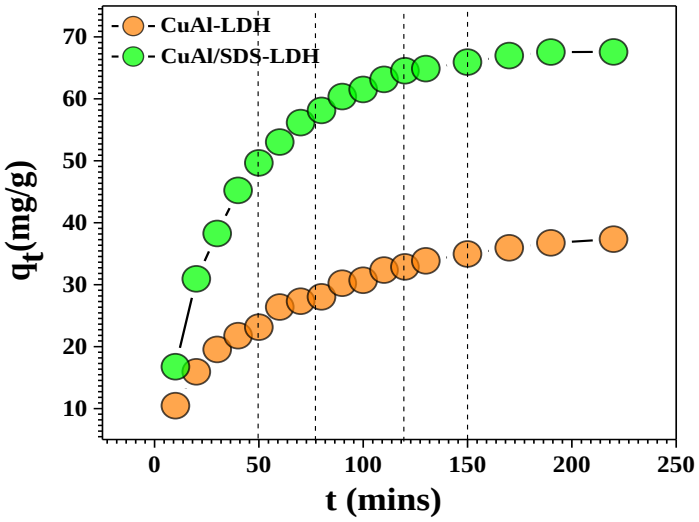

Fig III.13: Effect of contact time on the adsorption capacities of CuAl-LDH and CuAl/SDS-LDH (Initial dye concentration = 60 mg/L, pH = neutral, adsorbent dosages = 44 mg, volume = 50 mL).

III.3.3.5. Effect of solution pH

Another essential parameter that influences the adsorption process is the solution pH, and it can also affect the liquid phase chemistry and binding sites of LDH surface. The effect of pH during the adsorption process was observed in the range of 4-10, which is shown in **Fig III.14.** It is seen that for CuAl-LDH and CuAL/SDS-LDH under acidic pH-4, the highest adsorption, up to 86 % and 96.93 %, respectively, was achieved while moving towards the basic pH-10, which denotes a lower amount of dye retained on the surface of the adsorbent. Under alkaline conditions, the increase in concentration of OH^- ions competes with anionic methyl red dyes for the positively charged vacant sites, and simultaneously, the positively charged surface of the adsorbent also gets reduced. As a result, at high pH value, adsorption capacity is low. On the contrary, at low pH the existence of additional H^+ ion that accumulated over the LDH surface imparts a large positive charge that can easily interacts with anionic dyes and favors greater intake.[28] From the result displayed in **Fig III.14**, it can be concluded that within the examined pH range (4-10), the surfactant-modified LDH can enhance the greater removal of dye compare to unmodified LDH. At pH below 4, generally the structure of LDH gets destroyed, which could decrease the sorption

capacity for methyl red. However, the main factor contributing to the adsorption of methyl red dye on pristine LDH and CuAl/SDS-LDH may be explained by the electrostatic forces of attraction between positively charged LDH surfaces and negatively charged anionic dye.[20] Since the chemical structure of methyl red possesses carboxy ($-COO^-$) group, which can be easily attracted to the positively charge adsorption site. From the theoretical consideration, the point of zero charge value (PZC) can provide an optimum pH value for better adsorption of dyes. In general, if the solution pH is less than PZC, then the adsorbent will prefer anionic dyes, whereas for pH>PZC, the adsorbent shows greater adsorption for cationic dyes.[55]

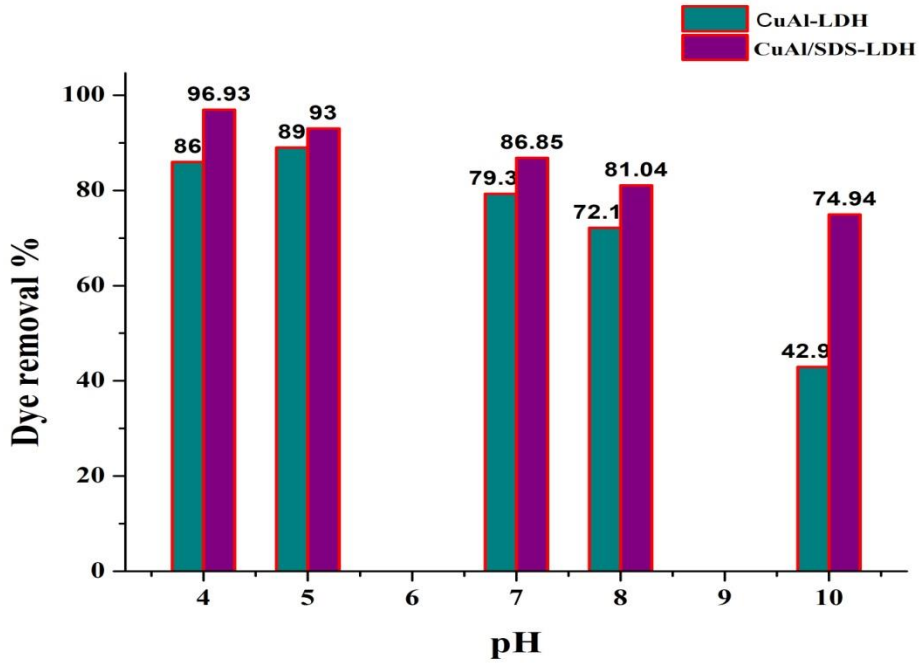

Fig III.14: Effect of solution pH on the adsorption efficiency of methyl red dye by two adsorbents (Initial concentration = 95 mg/L, volume = 20 mL, contact time = 2 hour, catalyst dosages = 22 mg).

III. 3.3.6. Mechanism of adsorption

The adsorption behavior of the methyl red dye on both CuAl-LDH and CuAl/SDS-LDH follows pseudo-second-order kinetics. Considering the adsorption capacity, this kinetic model envisages the nature of adsorption throughout the entire concentration of dye solution and supports chemisorption as the rate-determining mechanism. Generally, most of the LDH material exhibits important characteristics like high surface area, high porosity, and exchangeable ions,

which may account for the extraction of different anionic dye species from its aqueous solution. Moreover, the main factor responsible for the adsorption process can be attributed to highly positive charged density on LDH layers and the stronger interactions between incoming anionic dyes and LDH.[56] Besides, modification with the surfactants molecules creates a partitioning medium on both the internal and external surfaces of CuAl/SDS-LDH, which can improve the hydrophobic nature of LDH particles. This organic medium is essential and preferably increases the interaction among organic dyes and organo-modified LDH, and it also acts as a partitioning medium for contaminants. However, the adsorption process involves an intricate mechanism, and it may be due to a combination of several possible interactions, such as vander Waals force, H-bonding, electrostatic attraction, and the partitioning effect.[20,53] To further investigate the adsorption process, the analysis of FTIR spectrum displayed in **Fig III.2** clearly confirms the adsorption of dye.

III.3.3.7. Reusability

Reusability performances can reveal the efficacy of the material by using the same adsorbent repeatedly for industrial application; therefore, it is important to determine the economic feasibility of the adsorbents. The reusability experiment displayed in **Fig III.15** for the pristine LDH and surfactant-modified CuAl/SDS-LDH was examined up to the fourth cycle on 60 mg/L methyl red dye at neutral pH and 22 mg of adsorbent dosages. The initially adsorbed methyl red dye on the surface of the adsorbent was removed after each cycle by washing in a solvent acetone, which is then dried at room temperature. For CuAl/SDS-LDH, the percentage of dye removal efficiency declines after every consecutive cycle, and in the first cycle, the removal efficiency reached up to 98 %, which then continuously decreases to 28.86 % in the last cycle. In case of CuAl-LDH, the removal percentage is comparatively lower and lies between 72.36 and 28.86 %. The gradual decreases in dye adsorption capacity can be attributed to the loss of active adsorption sites due to the destruction of the structure of surfactant-loaded LDH.[57]

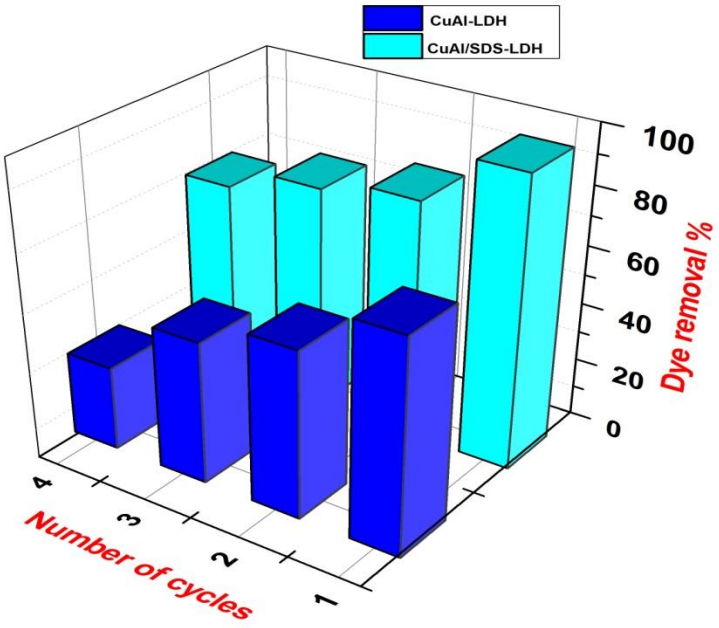

Fig III.15: Reusability studies for the removal efficiency of methyl red dye over two adsorbents (Initial dye concentration = 60 mg/L, adsorbent dosages = 22 mg, pH = neutral, contact time = 12 hours).

III.4. Conclusions

The study suggests that both the adsorbents CuAl-LDH and surfactant-modified CuAl/SDS-LDH can be easily synthesized and showed excellent efficiency for the removal of targeted anionic dyes. The results obtained from the physicochemical characterization infer the mesoporous nature, crystallinity, and the expected elemental compositions of the materials without impurity. However, the adsorption isotherm and kinetics data are well fitted according to Langmuir and pseudo-second-order kinetic models. The CuAl/SDS-LDH indicates a higher intake of organic dye pollutant with the maximum monolayer adsorption capacity q_{max} = 411 mg/g compare to CuAl-LDH (q_{max} = 209 mg/g). The influence of temperature on the adsorption activity exhibits spontaneous and endothermic process. The adsorbents can be reuse up to fourth cycle. Therefore, modification with the surfactants in the present materials has shed light on the need for emerging researchers for further investigate of the surfactants-fabricated LDH-based adsorbents.

III.5. References

1. F. Lu, D. Astruc, *Coord. Chem. Rev*., 356, **2018**, 147-164.
2. A.A. Peláez-Cid, A.M. Herrera-González, M. Salazar-Villanueva, A. Bautista-Hernández, *J. Env. Manag*., 181, **2016**, 269-278.
3. L. Wang, A. Wang, *J. Hazard. Mater*.,147, **2007**, 979-85.
4. A.S. Özcan, B. Erdem, A. Özcan, *Colloids Surf. A Physicochem. Eng.* 266, **2005**, 73-81.
5. Y. Badr, M.G. Abd El-Wahed, M.A. Mahmoud, *J. Hazard. Mater*., 154, **2008**, 245-53.
6. B. Lellis, C.Z. Fávaro-Polonio, J.A. Pamphile, J.C. Polonio, *Biotechnology. Res. Innov*., 3, **2019**, 275-90.
7. Z. Yang, F. Wang, C. Zhang, G. Zeng, X. Tan, Z. Yu, H. Wang, F. Cui, *RSC Adv.*, 6, **2016**, 79415-79436.
8. A.Y. Zahrim, N. Hilal, *Water Resource. Ind.*, 3, **2013**, *3*, 23-34.
9. C. Sahoo, A.K. Gupta, A. Pal, *Desalination*., 181, **2005**, 91-100.
10. Q. Wang, A. Tang, L. Zhong, X. Wen, P. Yan, *Powder Technol.*, 339, **2018**, 872-881.
11. N. Al-Bastaki, *Chem. Eng. Process.*, 43, **2004**, 1561-1567.
12. A.Y. Zahrim, C. Tizaoui, N. Hilal, *Sep Sci Technol*., 46, **2011**, 883-892.
13. I.M. Ahmed, M.S. Gasser, *Appl. Surf. Sci*., 259, **2012**, *259*, 650-656.
14. Z. Zaheer, A.A. Aisha, E.S. Aazam, *J. Mol. Liq.*, 283, **2019**, *283*, 287-298.
15. A.S. Eltaweil, E.M. Abd El-Monaem, G.M. El-Subruiti, M.M. Abd El-Latiff, A.M. Omer, *RSC Adv.* 10, **2020**, 19008-19019.
16. G. Mishra, B. Dash, S. Pandey, *Appl. Clay. Sci*., 153, **2018**, 172-186.
17. Y.X. Chen, R. Zhu, Z.L. Xu, Q.F. Ke, Q. Zhang, Y.P. Guo, *J. Mater. Chem. B*., 5, **2017**, 2245-2253.
18. Y. Jiang, Z. Hao, H. Luo, Z. Shao, Q. Yu, M. Sun, Y. Ke, Y. Chen, *RSC Adv.*, 8, **2018**, 11078-11086.
19. P. Wu, T. Wu, W. He, L. Sun, Y. Li, D. Sun, *Colloids Surf. A Physicochem. Eng. Asp.*, 436, **2013**, *436*, 726-731.
20. B. Zhang, Z. Dong, D. Sun, T. Wu, Y.J. Li, *J. Ind. Eng. Chem*., 49, **2017**, 208-218.
21. J. Li, S. Zhang, Y. Chen, C. Liu, X. Zhang, M. Yi, *RSC Adv.*, 46, **2017**, 29051-29057.
22. J. Qu, X. He, Z. Lei, Q. Zhang, X. Liu, *Solid State Sci*., 74, **2017**, 125-130.
23. M. Meyn, K. Beneke, G. Lagaly, *Inorg. Chem.*, 29, **1990**, 5201-5207.
24. N. Iyi, K. Tamura, H. Yamada, *J. Colloid Interface Sci*., 340, **2009**, 67-73.
25. S. Berner, P. Araya, J. Govan, H. Palza, *J. Ind. Eng. Chem*., 59, **2018**, 134-140.
26. M.A.M. El-Mansy, I.S. Yahia, *Spectrochim. Acta A*., 130, **2014**, 59-63.
27. G. Rathee, N. Singh, R. Chandra, *ACS Omega*., 5, **2020**, 2368-2377.
28. Y. Chen, C. Jing, X. Zhang, D. Jiang, X. Liu, B. Dong, L. Feng, S. Li, Y. Zhang, *J. Colloid Interface Sci.*, 548, **2019**, 100-109.
29. S. Natarajan, R. Naresh, V. Thiagarajan, *Chemistry Select.*, 5, **2020**, 4165-4174.
30. I. Mindru, D. Gingasu, L. Patron, G. Marinescu, J.M. Calderon-Moreno, S. Preda, O. Oprea, N. Sultana, *Ceram. Int*., 42, **2016**, 154-164.
31. S. Lei, S. Wang, B. Gao, Y. Zhan, Q. Zhao, S. Jin, G. Song, X. Lyu, Y. Zhang, Y. Tang, *J. Colloid Interface Sci*., 577, **2020**, 181-190.

32. R. González-Olevera, C.I. Urquiza-Castro, G.E. Negrón-Silva, D. Ángeles-Beltrán, L. Lomas-Romero, A. Gutiérrez-Carrilo, V.H. Lara, R. Santillan, J.A. Morales-Serna, *RSC Adv.*, 6, **2016**, 63660-63666.
33. R. Dutta, T.V. Nagarjuna, S.A. Mandavgane, J.D. Ekhe, *Ind. Eng. Chem. Res.*, 53, **2014**, 18558-18567.
34. I. Langmuir, *J. Am. Chem. Soc.*, 40, **1918**, 1361-1403.
35. G. Rathee, A. Awasthi, D. Sood, R. Tomar, V. Tomar, C. Chandra, *Sci Rep*., 9, **2019**, 16225.
36. H. Freundlich, *J. Phys. Chem*., 57, **1906**, 385-471.
37. M.I. Temkin, V. Pyzhev, V. *Acta Physiochimica URSS.* 12, **1940**, 327-356.
38. D.F. Rhomdhane, Y. Satlaoui, A. Charef, R. Azouzi, *Journal of Chemistry*., 17, **2020**, 4376173.
39. M. Ghaedi, R. Hassani, K. Dashtian, G. Shafie, M.K. Purkait, H. Dehghan, *Desalination and Water Treat*., 57, **2016**, 22646-22654.
40. S. Dadfarnia, A.M. Shabani, S.E. Moradi, S. Emami, *Appl. Surf. Sci.*, 330, **2015**, 85-93.
41. E.A. Khan, Shahjahan, T.A. Khan, *J. Mol. Liq.*, 249, **2018**, 1195-1211.
42. M.A. Ahmad, N. Ahmad, O.S. Bello, *Appl. Water Sci.*, 5, **2015**, 407-423.
43. E. Yilmaz, E. Sert, F.S. Atalay, *J. Taiwan Inst. Chem. Eng*., 65, **2016**, 323-330.
44. S. Lagergren, *Kungl. Svenska Vetenskapsakad. Handl*., 24, **1898**, 1-39.
45. Y.S. Ho, G. Mckay, *Chem. Eng. J*., 70, **1998**, 115-124.
46. W.J. Weber, J.C. Morris, *J. Sanit. Eng. Div*., 89, **1963**, 31-60.
47. P. Patanjali, A. Mandal, I. Chopra, R. Singh, *Int J Environ Anal Chem.*, 100, **2020**, 1-23.
48. H. Zaghouane-Boudiaf, M. Boutahala, L. Arab, *Chem. Eng. J*., 187, **2012**, 142-149.
49. T. Kameda, E. Kondo, T. Yoshiaki, *Sep. Purif. Technology*., 122, **2014**, 12-16.
50. J. Huang, Y. Liu, X. Wang, *J. Hazard. Mater*., 160, **2008**, 382-387.
51. D. Zhao, S. Guodong, J. Hu, C. Chen, X. Wang, *Chem. Eng. J*., 171, **2011**, 167-174.
52. B.S. Inbaraj, C.P. Chiu, G.H. Ho, J. Yang, B.H. Chen, *J. Hazard. Mater.*, 137, **2006**, 226-234.
53. Y. Chun, G. Sheng, S.A. Boyd, *Clays Clay Miner*., 51, **2003**, 415-420.
54. D.F. Enache, E. Vasile, C.M. Simonescu, A. Răzvan, A. Nicolescu, A.C. Nechifor, O. Oprea, R.E. Pătescu, C. Onose, F. Dumitru, *J. Solid State Chem*., 253, **2017**, 318-328.
55. J. Hong, Z. Zhiliang, L. Hongtao, Q. Yanling, *RSC Adv.*, 4, **2014**, 5156-5164.
56. R.R. Shan, L.G. Yan, Y.M. Yang, K. Yang, S.J. Yu, H.Q. Yu, B.C. Zhu, B. Du, *J Ind Eng Chem*., 21, **2015**, 561-568.
57. D. Brahma, H. Saikia, *Inorg. Nano-Met. Chem*., 53, **2023**, 605-620.